# UNIQUE FEATURES OF THE J-PARC LINAC AND ITS PERFORMANCE - LESSONS LEARNT

A. Ueno#, J-PARC, JAEA, Tokai, Naka, Ibaraki, 319-1195, Japan

*Abstract*

The J-PARC (Japan Proton Accelerator Research Complex) linac has been successfully commissioned up to its design energy of 181MeV and almost the first stage design peak intensity of 30mA. The following unique methods and hardware features adopted in the J-PARC linac are explained and those results are presented in this paper. The surface production dominating Cs-free $H^-$ IS (Ion Source) with magnetic focus LEBT (low energy beam transport), macro-beam-pulse shaping method related with the J-PARC 30mA-RFQ (Radio Frequency Quadrupole linac) design, a stable one-shot operation method, beam suspending method for machine protection, RF-chopper system related with the operation parameter of the RFQ, one-turn injection into the following J-PARC RCS (Rapid Cycling Synchrotron), transverse matching using TRACE3D PMQ (Permanent Magnet Quadrupole) elements approximating the fringe field effects of the electro-quadrupole magnets, PR (Periodic Reverse) electroforming for high-duty compact DTQ (Drift Tube Quadrupole) coil and thick pure plating of DTL (Drift Tube Linac) and SDTL (Separated-type DTL) and 2 cavity behaviour of SDTL fed with one Klystron.

## OVERVIEW OF J-PARC LINAC

As shown in Fig. 1, the J-PARC linac consists of 34 accelerating cavities (RFQ, DTL1~3, SDTL1A~15B), IS, LEBT, MEBT1 (Medium Energy Beam Transport 1) and beam transport to RCS [1]. Since the uncoupled SDTLnA and B (n=1~15) are fed RF-power by one klystron, 19 klystrons are used for acceleration. At the J-PARC first stage, the J-PARC linac accelerates an $H^-$ beam with a peak intensity of 30mA up to the energy of 181MeV with a pulse width of 500μs and a repetition rate of 25Hz.

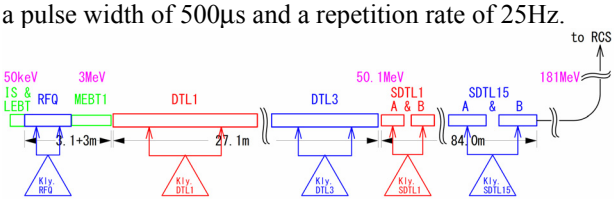


Figure 1: Scheme of J-PARC linac.

## SURFACE PRODUCTION DOMINATING CS-FREE IS & MAGNETIC FOCUS LEBT

In almost all of IS's for high intensity $H^-$ accelerators, Cs is seeded on PE (Plasma Electrode) in order to increase $H^-$ production efficiency. Since the thickness of the Cs layer affects to the efficiency greatly, it is not so easy to keep $H^-$ intensity constant with the Cs seeded $H^-$ IS. Also the frequency of sparking in high-voltage gaps of IS or RFQ is increased by the Cs. For stable operation, Cs-free IS is adopted for J-PARC. In order to minimize emittance growth by using SCN (Space-Charge Neutralization) measured as more than 90% [2], the magnetic focus LEBT composed of two solenoid and one ejection angle correction magnets is adopted. A schematic drawing of the IS and LEBT is shown in Fig. 2.

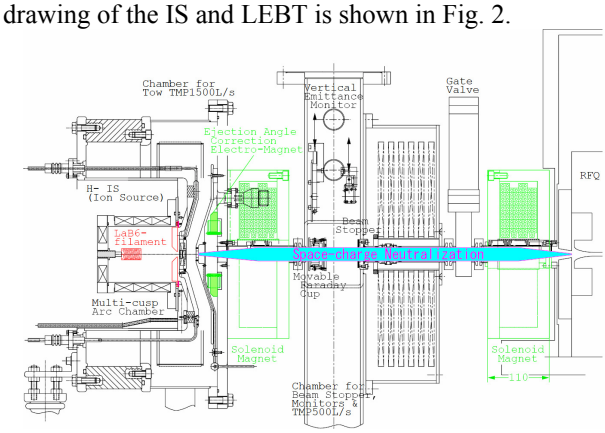


Figure 2: Schematic drawing of IS and LEBT.

On 1995, in a Cs-free IS, a 16mA $H^-$ beam was produced by using a cylindrical arc-chomber (D150mm, L150mm), a $LaB_6$-filament, a PE shown as Fig.3(a) and an arc-current of 220A [3]. Although the plasma density was increased by using a smaller arc-chamber (D100mm, L125mm) and a higher arc-current of 290A, the intensity had been limited to 16mA by using the PE shown as Fig. 3(b), for two years. After the success of 4mA intensity increase by only increasing the temperature of PE with a thermal insulator ceramics flange shown as Fig. 3(c), various shapes of PE's shown in Fig. 3 were examined by the assumption of that surface $H^-$ production was dominating. Finally, a 38mA $H^-$ beam was produced by using PE shown as Fig.3(h) [4]. The $H^-$ production efficiency seems to be increased mainly by the deoxidization of PE surface made of Mo with the high temperature measured as about 500°C in $H_2$ gas.

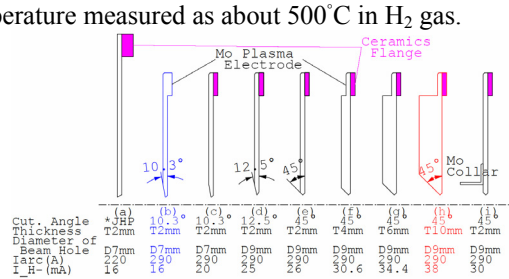


Figure 3: Various shapes of PE's examined.

## MACRO-BEAM-PULSE SHAPING & BEAM SUSPENDING METHODS

In order to avoid emittance rotation problem during the rise-time of SCN, macro-beam-pulse shaping by kicking the beam transversely is not available in magnetic focus

#akira.ueno@j-parc.jp

LEBT. Therefore, macro-beam-pulse is shaped by using RFQ longitudinal acceptance with modulating the injection energy in J-PARC. As shown in Fig. 4, RFQ acceleration starts after more than 100μs from IS arc pulse start and SCN established by low-energy unaccelerated beam transported through the LEBT. The end of macro-beam-pulse is determined by the end of RFQ-RF pulse since its fall-time is fastest. The macro-beam-pulse also ends by ending the RFQ-RF responding to MPS (Machine Protection System) fast interlock [5], for example DTL sparking and so on. In order to suspend beam acceleration for MPS reset time or one-shot operation, only IS arc pulse timing is delayed 0.2 ms after RFQ-RF pulse end where IS extraction voltage is switched off. As shown in Fig.5, no acceleration was observed for the beam with 10keV lower energy than the design energy of 50keV. IS signals {potential, arc voltage, arc current, $H^-$ beam measured by FC(Faraday Cup)} and RFQ RF-field are shown in Fig. 6.

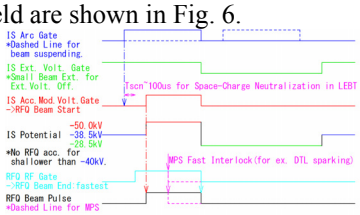


Figure 4: Timing-Chart of J-PARC IS & RFQ.

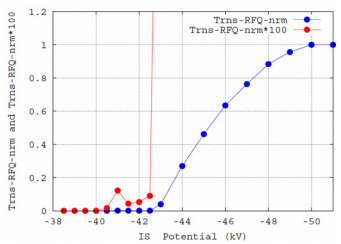


Figure 5: Measured Relationship between IS Potential and RFQ Transmission.

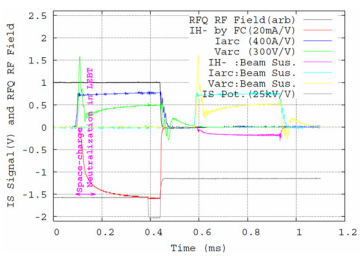


Figure 6: IS Signals and RFQ RF Field.

## *J-PARC 30mA-RFQ Design and Manufacturing*

In order to make the above macro-beam-pulse shaping available and the RFQ as emittance filter in both longitudinal and transverse motions, the RFQ is designed by using codes KEKRFQ [6] and PARMTEQm [7]. By using KEKRFQ, longitudinal and transverse acceptances including space-charge effect are kept constant in GB (Gentle Buncher) section (synchronous phase $\phi_s = -88^\circ \rightarrow -30^\circ$) and accelerator section ($\phi_s = -30^\circ$), respectively. The designed cell parameters of energy, modulation factor 'm', minimum bore radius 'a' and $\phi_s$ are shown as the functions of longitudinal position in Fig. 7(a). Since 'm' and 'a' change rather rapidly in GB, the accelerating field should be as accurate as possible. The approximated accelerating field used in PARMTEQm is shown as Eq. (1) whose parameters are explained in Fig. 7(b). In the equation, incorrect cell length Lc(i+1) is used to calculate A(i+1). The accelerating field is more accurately approximated by using Eq. (2). In order to stabilize the accelerating quadrupole field of the RFQ against the dipole-mode mixing, PILS's (π-mode Stabilizing Loops) are installed in the RFQ as shown in Fig. 8(a) [8, 9]. The electric field near beam axis is modified as shown in Fig. 8(b), in which the field distribution of one PISL cell length between pares of vertical and horizontal PISL rods calculated by MAFIA [10] are shown.

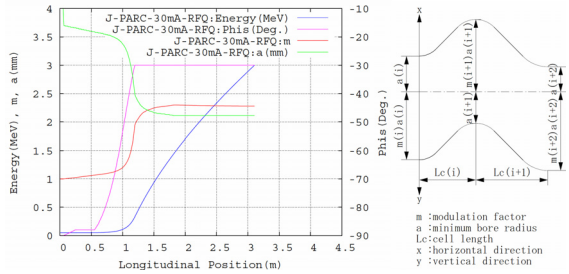


(a) (b)

Figure 7: (a) Designed Cell Parameters and (b) Explanation of 'a', 'm' and 'Lc'.

$$E_z(z) = \{A(i) + \frac{A(i+1) - A(i)}{L_c(i)} dz\} e(L_c(i), z) \quad \text{where} \quad A(i) = \frac{m(i)^2 - 1}{m(i)^2 I_0(\frac{\pi a(i)}{L_c(i)}) + I_0(\frac{\pi m(i) a(i)}{L_c(i)})} \quad (1)$$

$$E_z(z) = \{A_0(i) + \frac{A_1(i) - A_0(i)}{L_c(i)} dz\} e(L_c(i), z) \quad \text{where} \quad A_0(i) = \frac{m(i)^2 - 1}{m(i)^2 I_0(\frac{\pi a(i)}{L_c(i)}) + I_0(\frac{\pi m(i) a(i)}{L_c(i)})},$$

$$\text{and} \quad A_1(i) = \frac{m(i+1)^2 - 1}{m(i+1)^2 I_0(\frac{\pi a(i+1)}{L_c(i)}) + I_0(\frac{\pi m(i+1) a(i+1)}{L_c(i)})} \quad (2)$$

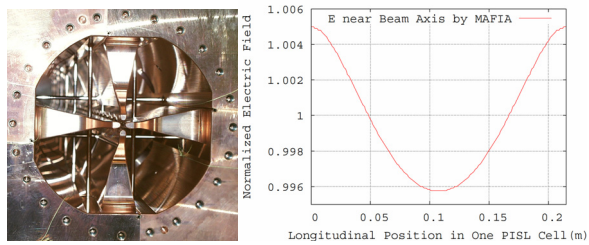


(a) (b)

Figure 8: Inside View of RFQ and Field Distribution near Beam Axis in One PISL Cell Calculated by MAFIA.

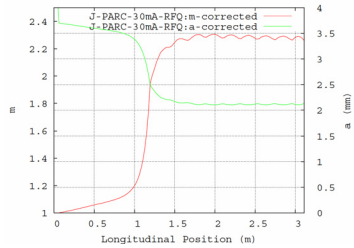


Figure 9: 'm' and 'a' for Design Accelerating Field.

The RFQ was manufactured with corrected 'm' and 'a' shown in Fig. 9.

## RF-CHOPPER & RFQ OPERATION PARAMETER SUITABLE FOR IT

In Figs. 10 and 11, the schematic drawing of MEBT1 and the inside-view of 2 coupled RF-chopper cavities are shown. Beam is deflected and dumped on a movable scraper made of graphite by the RF-field in RF-chopper. By switching RF-power to the RF-chopper, it is possible to produce arbitrary width and number of intermediate-beam-pulses [11, 12, 13]. Although the range of 3MeV-$H^-$ beam is very short (a few μm) and therefore energy density depositing on it is very high, it is confirmed experimentally that graphite stands for design beam duty (30mA*270μs*25Hz) of the J-PARC first stage.

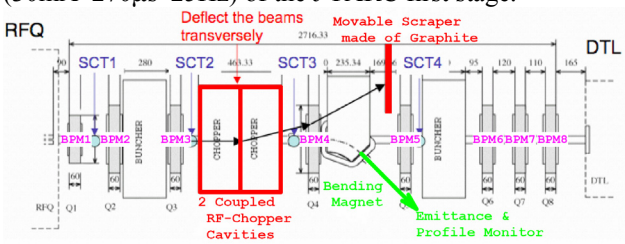


Figure 10: Schematic Drawing of MEBT1.

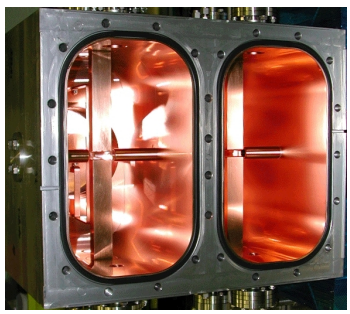

Figure 11: Inside View of RF-Chopper Cavities.

The 'remaining beam' which is deflected by the RF-chopper but undumped and accelerated by the following accelerators should be reduced as small as possible, in order to reduce residual radiation in the RCS. Early in the J-PARC linac commissioning, it was difficult to reduce the 'remaining beam' lower than measurement accuracy especially for high peak intensity beam about 30mA. In order to minimize the longitudinal halo of the beam accelerated with the RFQ, RFQ RF-field and IS potential are searched to minimize the horizontal beam size at the position with dispersion downstream of the bending magnet in MEBT1. The result is shown in Fig. 12.

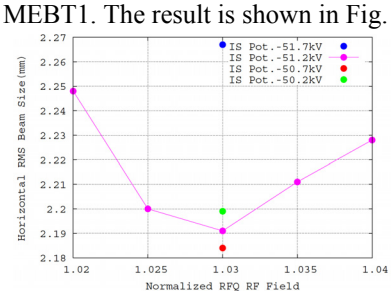


Figure 12: Relationship between RFQ RF-Field & IS Potential and Horizontal RMS Beam Size at Position with Dispersion.

By setting the RFQ RF-field at 3% higher than the design value and the IS potential at –50.7kV, the 'remaining beam' can be reduced lower than the measurement accuracy of linac monitor. By using RCS BLM (Beam Loss Monitor) [14] at the position with dispersion, the 'remaining beam' can be measured most accurately as shown in Fig. 13 in which very slight beam is measured (red line), although all of the beam is deflected by the RF-chopper. The 'remaining beam' due to longitudinal halo will hopefully be eliminated by RF-chopper with half resonant frequency of 162MHz.

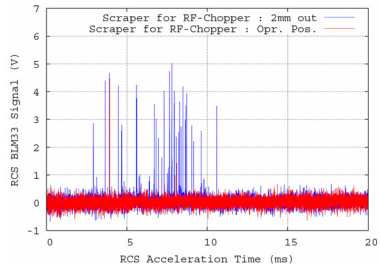


Figure 13: BML Signal during RCS Acceleration Time at Position with Dispersion.

The measured LEBT and MEBT1 SCT signals and RFQ RF-field are shown in Fig. 14. The rise-time of the macro-beam-pulse (blue line) measured by MEBT1-SCT3 (upstream of RF-chopper) is rather short (about 3μs) which is the proof of SCN establishment in the LEBT. The fall-time is much faster than it (about 1μs) since it is determined by 80% of the RFQ RF-field (black line). Two type of chopped beam measured by MEBT1-SCT5 (downstream of RF-chopper) are shown with green (112ns, 22turn) and red (560ns, 1turn) lines artificially.

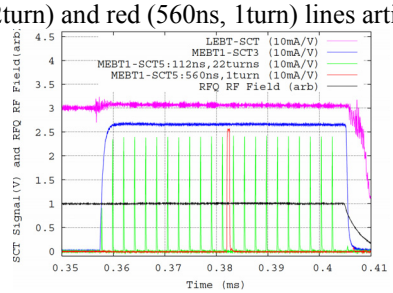


Figure 14: LEBT and MEBT1 SCT Signals and RFQ RF-Field.

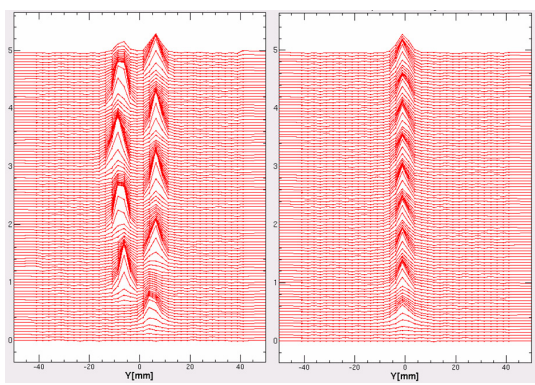


(a) (b)

Figure 15: Mountain Plots of RCS Vertical IPM Signals before (a) and after (b) Injection Error Correction.

One turn injection into the RCS makes injection error correction possible. The beam position and profile measured by an RCS IPM (residual gas Ionization Profile Monitor) as mountain plots during the first 9turns are shown in Fig. 15(a)(before correction) and (b)(after correction).

The RF-field in the RF-chopper, MEBT1-BPM right and left signals are shown as red, blue and green lines, respectively in Fig. 16. The ringing of RF-field at RF on/off transient-time due to RF-power flow between the 2 coupled cavities is observed. The shit of beam position due to the ringing is also observed for about 50ns after beam rise-time. If the affect of the ringing is significant, it can be eliminated by driving each RF-chopper cavity independently with two RF-sources.

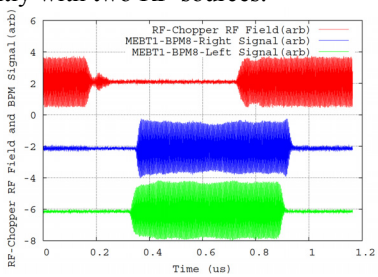


Figure 16: RF-Chopper RF-Field and Right- and LEFT-BPM Signals of MEBT1.

## TRANSVERSE MATCHING WITH TRACE3D PMQ APPLOXIMATION

As reported in the paper of LINAC2002 [17], the fringe field of Q(quadrupole)-magnets should be taken into account. By using 20-pieces of hard-edge magnets (red line of Fig. 17) for each Q-magnet, the ellipses measured in the MEBT1 test setup are reproduced.

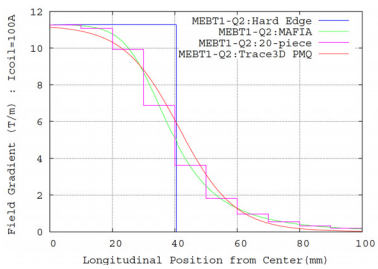


Figure 17: Various Field Distributions of MEBT1-Q2 Used for TRACE3D Calculations.

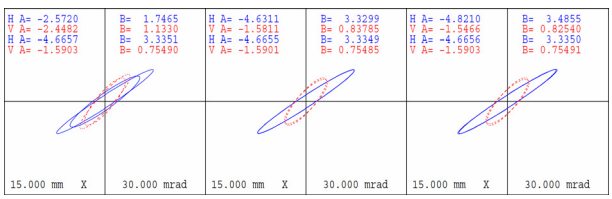


(a) (b) (c)

Figure 18: Measured and Calculated Ellipses in MEBT1 Test by Using Hard Edge Field (a), 20-Pieces Field (b) and TRAC3D PMQ Field (c).

Instead of 20-pieces of hard-edge magnets, PMQ element (magenta line of Fig. 17) of TRACE3D [18] can also reproduce the experimental result as shown in Fig. 18(c). In Fig. 18(a), (b) and (c), measured and calculated ellipses are shown for hard-edge field, 20-pieces field and PMQ field, respectively. Since online control of the J-PARC linac is done by using XAL [19], the PMQ element has been transplanted into XAL [20]. All of Q-magnets in J-PARC linac are treated as PMQ elements.

## DTQ-COIL & CAVITY-PLATING USING PR-ELECTROFORMING

PR(Periodic Reverse)-electroforming, in which electroforming and short electro-polishing is reiterated without any brightening agent, is able to produce thick and pure plating comparable with OFC (Oxygen Free Copper). Compact DTQ-coil shown in Fig. 19(a) was produced with it and is able to be operated with high magneto-motive-force and high-duty (3.5turn, 600A, DC) [21]. As shown in Fig. 19(b), each inside of DTL or SDTL cavity was plated with PR-electroforming. All of DTL and SDTL cavities were successfully high-power RF-conditioned up to 20% higher powers of the design values. [22, 23]

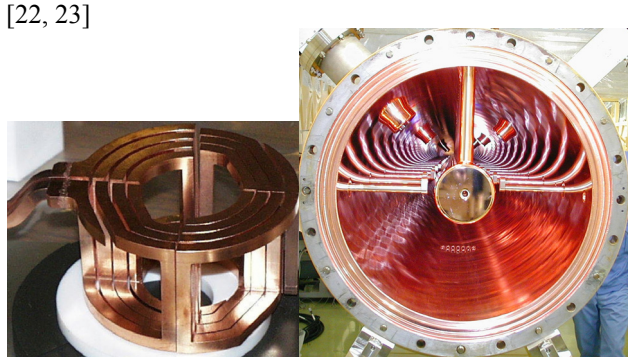

(a) (b)

Figure 19: Photos of DTQ-Coil (a) and Inside View of DTL1 (b).

## 2 CAVITY BEHAVIOR OF SDTL

Each pair of SDTLnA and B (n=1~15) is driven by one klystron. The vector-sum of the two RF-fields is feedback-controlled [24]. However, unexpectedly high RF-field unbalances caused by beam loading are observed in several of the pairs. In Fig. 20, the measured maximum (SDTL03) and minimum (SDTL12) unbalances are shown when a 28mA-beam with 100ms pulse width is accelerated.

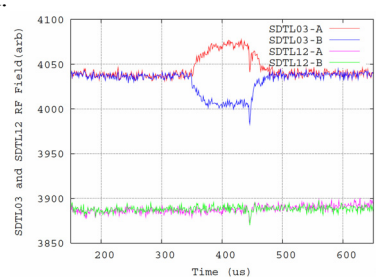


Figure 20: RF-Fields in SDTL03A&B and 12A&B while Accelerating 28mA- and 100μs-Beam.

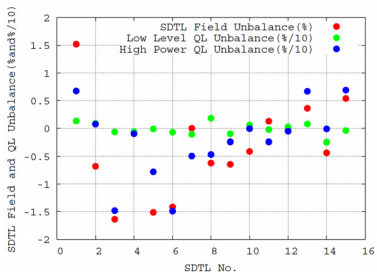


Figure 21:SDTL QL Unbalance (Preliminary) & RF-Field Unbalance while Accelerating 28mA- and 100μs-Beam.

In Fig. 21, the RF-field unbalance UBRF due to beam-loading and the QL (Loaded Q-value) unbalance UBQL calculated with following equations are shown.

UBRFn=(RFnA-RFnB)*2/(RFnA+RFnB)
UBQLn=(QLnA-QLnB)*2/(QLnA+QLnB)

In the latest beam acceleration, preliminarily, each QLnA and QLnB was measured by measuring RF decay-time during high-power operation as shown with blue circles in Fig. 21. The RF-field unbalance due to beam-loading seems to have some relationship with the unbalance of the high-power loaded Q-value, although more accurate measurements are necessary. If the change of the loaded Q-value is correct, multipacting is one candidate of the causes.

## SUMMARY

The following unique methods and hardware features adopted in the J-PARC linac are explained and the performances and problems of them are presented.

- Surface production dominating Cs-free $H^-$ IS
- succeeded in produce more than 30mA stably.
- Macro-beam-pulse shaping by using RFQ longitudinal acceptance with magnetic focus LEBT
- succeeded in producing the pulse with rather high rise- and fall-time. It also makes possible stable one shot operation, fast beam suspending for MPS and so on.
- RF-chopper
- succeeded in reducing the 'remaining beam' lower than the measurement accuracy of linac monitor by searching the RFQ operation parameter. One turn injection with it into the following RCS is essential for injection error correction. Two RF-sources are necessary to eliminate the measured RF-ringing. The RF-chopper with half resonant frequency of 162MHz will eliminate the 'remaining beam' and makes possible beam intensity double by inevitably used two scrapers.
- Transverse matching with TRACE3D PMQ
- succeeded in representing the fringe field effects. All of Q-magnets in the J-PARC linac are treated as PMQ in XAL and TRACE3D.
- PR (Periodic Reverse) electroforming.
- succeeded in producing high-duty compact DTQ-coil and thick pure plating of DTL and SDTL.
- 2 cavity behaviour of SDTL fed with one Klystron.
- unexpectedly high RF-field unbalance between the 2 cavities are observed. The RF-field unbalance due to beam-loading seems to have some relationship with the unbalance of the high-power loaded Q-value (preliminarily measured).

## REFERENCES

[1] K. Hasegawa, Proc. of PAC2007, 2619(2007).
[2] S. Fujimura and A. Ueno, Proc. of LINAC1996, 343(1996).
[3] A. Ueno et al., Proc. of LINAC1996, 293(1996).
[4] A. Ueno et al., Rev. Sci. Instrum. 75, 1714(2004).
[5] H. Sakaki et al., Proc. of APAC2004, 622(2004).
[6] A. Ueno and Y. Yamazaki, Proc. of LINAC1990, LA-12004-C, 329(1991).
[7] K. R. Crandall et al., LA-UR-96-1836, (1998).
[8] A. Ueno and Y. Yamazaki, Nucl. Instr. and Meth. A300, 15(1991).
[9] A. Ueno and Y. Kondo, Proc. of LINAC2000, 545(2000).
[10] T. Weiland, Part. Accel., 17, 227, (1985).
[11] S. Fu and T. Kato, Nucl. Instr. And Meth. A 440, 296(2000).
[12] S. Wang, S. Fu and T. Kato, Proc. of LINAC2004, 770(2004).
[13] T. Kato et al., Proc. of PAC2003, 1455(2003).
[14] K. Yamamoto et al., Proc. of EPAC2008, 382(2008).
[15] K. Satou et al., Proc. of EPAC2008, 1275(2008).
[16] H. Hotchi, "Status of J-PARC Commissioning", Proc. of ICFA-HB2008.
[17] A. Ueno et al., Proc. of LINAC2002, 356(2002).
[18] K. R. Crandall and D. P. Rusthoi, LA-UR-97-886, (1997).
[19] J. Galambos, et al., Proc. of ICALEPCS2003, 332(2003).
[20] C. K. Allen, et al, Proc. of PAC2007, 218(2007).
[21] K. Yoshino et al., Proceedings of LINAC2000, 569(2000).
[22] H. Ino et al., Proceedings of LINAC2000, 1015(2000).
[23] F. Naito, Proc. of APAC2007, 1(2007).
[24] T. Kobayashi et.al., Proceedings of PAC2007, 2128(2007).

### *Acknowledgement*

The author express sincere thanks to the members of J-PARC linac and RCS for their works.